Simultaneous description of conductance and thermopower in single-molecule junctions from many-body ab initio calculations

Jin, Chengjun; Markussen, Troels; Thygesen, Kristian Sommer

Published in:
Physical Review B

Link to article, DOI:
10.1103/PhysRevB.90.075115

Publication date:
2014

Document Version
Publisher's PDF, also known as Version of record

Simultaneous description of conductance and thermopower in single-molecule junctions from many-body *ab initio* calculations

Chengjun Jin, Troels Markussen, and Kristian S. Thygesen*

Center for Atomic-scale Materials Design, Department of Physics, Technical University of Denmark, DK-2800 Kgs. Lyngby, Denmark

(Received 28 June 2014; revised manuscript received 28 July 2014; published 11 August 2014)

We investigate the electronic conductance and thermopower of a single-molecule junction consisting of bis-(4-aminophenyl) acetylene (B4APA) connected to gold electrodes. We use nonequilibrium Green's function methods in combination with density-functional theory (DFT) and the many-body GW approximation. To simulate recent break junction experiments, we calculate the transport properties of the junction as it is pulled apart. For all junction configurations, DFT with a standard semilocal functional overestimates the conductance by almost an order of magnitude, while the thermopower is underestimated by up to a factor of 3, except for the most highly stretched junction configurations. In contrast, the GW results for both conductance and thermopower are in excellent agreement with experiments for a wide range of electrode separations. We show that the GW self-energy not only renormalizes the molecular energy levels but also the coupling strength. The latter is a consequence of the finite response time associated with the electronic screening in the metal electrodes.

DOI: 10.1103/PhysRevB.90.075115 PACS number(s): 73.63.−b, 73.40.Gk, 85.65.+h

I. INTRODUCTION

Molecular junctions consisting of a single molecule connected to metallic electrodes via atomically well-defined chemical bonds represent unique benchmark systems for the study of charge, spin, and heat transport at the nanoscale [1]. Fascinating quantum phenomena such as giant magnetoresistance [2], Kondo effects [3,4], and quantum interference [5,6] have recently been reported for single-molecule junctions. Moreover, these systems allow for detailed studies of charge transfer and energy level alignment at metal-molecule interfaces of great relevance to, e.g., organic electronic devices and dye-sensitized solar cells [7–10].

As an addition to standard charge transport experiments, thermopower measurements have recently been advanced as a powerful spectroscopic tool for single-molecule junctions [11–16]. The thermopower is directly related to the slope of the transmission function at the Fermi level and thus can be used to infer the carrier type, i.e., whether transport is n- or p-type (semiconductor language) or whether the transport takes place via the highest occupied molecular orbital (HOMO) or the lowest unoccupied molecular orbital (LUMO) (chemical language).

Both the conductance and thermopower are highly sensitive to the position and width of the molecular resonances in the junction. This poses a challenge for *ab initio* modeling of single-molecule junctions since a proper description of the level alignment at metal-molecule interfaces is known to be highly problematic within the popular framework of density functional theory (DFT) [17,18]. While it is in principle possible to obtain the correct conductance *or* thermopower of a single-molecule junction from a calculation with an incorrect level alignment (i.e., obtain the correct result for the wrong reason), it is much less plausible that a simultaneously good description of conductance *and* thermopower can be achieved unless the energy level alignment and level broadening are correctly described. Thus simultaneous modeling of the conductance and thermopower should represent a highly stringent test of the quality of the underlying electronic structure calculation.

Over the past decade, it has become clear that predictive and quantitatively accurate modeling of electronic energy level alignment and charge transport in metal-molecule junctions must be based on methods that go beyond the single-particle DFT description. The (self-consistent) GW approximation represents an accurate, although computationally demanding, alternative to DFT yielding quasiparticle (QP) energies in much better agreement with experiments. The improved description of the level positions is the main reason for the excellent agreement found between GW transport calculations and experiments on molecular junctions. However, in addition to the level alignment, the GW approximation accounts for two other effects, both of which are beyond the single-particle theories and which can have significant effects on the calculated transport properties. One is the change of the molecular wave functions arising from the interaction between the tunneling electron and its image charge in the electrode. This effect tends to contract the frontier orbitals toward the metal surface, and is stronger for molecules with large polarizability [19]. The second effect stems from the finite formation time of the image charge in the electrode represented roughly by the inverse of the plasmon frequency. This means that the image charge is "lacking behind" the tunneling electron and results in a reduction of the effective metal-molecule coupling strength [20]. Both of these effects are fully accounted for by the GW calculations presented in the present work, although only the latter is significant due to the relatively low polarizability of the bis-(4-aminophenyl) acetylene molecule (B4APA) studied here.

We have recently demonstrated that an excellent description of both the conductance and thermopower of benzenediamone (BDA) and benzenedicarbonitrile (BDCN) molecular junctions can be obtained using the GW method [21]. In contrast, standard DFT deviates from experiments by up to two orders of magnitude for these systems. Our previous work was based

*thygesen@fysik.dtu.dk

on a single (idealized) junction geometry, and the experimental data were taken from four independent experiments of conductance and thermopower for the two molecules, respectively. To establish a more faithful and consistent benchmarking of the GW approximation for electronic transport calculations, it is necessary to consider various junction geometries and preferentially compare to experiments where the conductance and thermopower were measured simultaneously. This is the motivation for the work reported in this paper.

Simultaneous measurements of conductance and thermopower of gold/B4APA were reported by Widawsky *et al.* [15]. The positive sign of the thermopower indicated that the electron transport through B4APA is hole-mediated, and this was supported by DFT-based transport calculations. It was shown that a correction of the DFT molecular energy levels was necessary in order to obtain a conductance and thermopower in agreement with experiments [15].

In this paper, we show that the conductance and thermopower of the gold/B4APA junction calculated with the GW approximation are in excellent agreement with the break junction experiments of Widawsky *et al.* Importantly, the good agreement is found for a wide range of stretching conditions. In contrast, DFT with a semilocal functional overestimates the conductance by a factor of 6 for all electrode separations while the thermopower is generally underestimated, except for very particular and highly stretched junction geometries. Secondly, we address the dynamical aspects of the image charge screening of the conductance and thermopower. Our calculations show that the finite response time of the electrode not only renormalizes the molecular energy levels, but also reduces the coupling strength between the molecule and the electrode. This effect reduces the conductance by almost a factor of 2 while the thermopower is essentially unaffected (in a one-level model, the thermopower is independent of the coupling strength).

II. METHODS

All the calculations were performed with the GPAW code [22] using the projector-augmented wave method. A bis-(4-aminophenyl) acetylene molecule (B4APA) is sandwiched between two Au tips attached to the Au(111) surface as illustrated in Fig. 1(a). The supercell contained eight 4×4 Au(111) atomic layers. The geometry of the molecule and Au tips was optimized until the residual force on every atom was below 0.02 eV/Å. For the structure optimization, we used the Perdew-Burke-Ernzerhof (PBE) exchange-correlation (xc) functional [23], and the first Brillouin zone was sampled on a $4 \times 4 \times 1$ k-point mesh.

The DFT and GW transport calculations were performed following the method described in Refs. [24,25]. The transmission function was calculated from the Landauer formula [26,27]

$$\mathcal{T}(E) = \mathrm{Tr}[G^r(E)\Gamma_L(E)G^a(E)\Gamma_R(E)], \tag{1}$$

where the retarded Green's function was obtained from

$$G^r(E) = \big[(E + i\eta)S - H_0 + V_{\mathrm{xc}} - \Delta V_H[G] - \Sigma_L^r(E) - \Sigma_R^r(E) - \Sigma_{\mathrm{xc}}[G](E)\big]^{-1}, \tag{2}$$

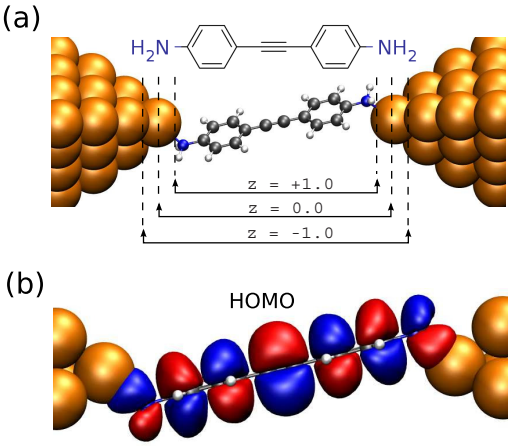

FIG. 1. (Color online) (a) A single bis-(4-aminophenyl) acetylene molecule (B4APA) is sandwiched between two Au tips attached to the Au(111) surface. The three different image plane positions used in the DFT+Σ method are indicated, namely $z = +1,0,-1$ Å relative to the Au tip atom. (b) Contour plot of the highest occupied molecular orbital (HOMO) of the B4APA molecule in the junction.

where S, H_0, and V_{xc} are the overlap matrix, the Kohn-Sham Hamiltonian matrix, and the PBE xc potential in the atomic orbital basis [28], respectively. η is a numerical positive infinitesimal which is set to 0.02 eV in the calculations. $\Sigma^r_{L/R}$ are the retarded lead self-energies and ΔV_H is the deviation of the Hartree potential from the equilibrium DFT-PBE value. Σ_{xc} is the many-body xc self-energy. For the HF and GW, Σ_{xc} is the nonlocal exchange potential and the GW self-energy, respectively. These self-energies are evaluated self-consistently. A standard non-equilibrium Green's function combined with density function theory (NEGF-DFT) calculation is recovered when Σ_{xc} is taken as the Kohn-Sham xc potential, V_{xc}. The self-consistent cycle is performed by a linear mixing of the Green functions. The energy-dependent quantities are represented on an energy grid ranging from -160 to 160 eV with an energy-grid spacing of 0.01 eV.

In the DFT+Σ method [21,29,30], the DFT energy levels of the molecule in the junction are corrected by two terms. First, a correction is added to the occupied and unoccupied orbitals, respectively, to account for the self-interaction error in the DFT energy levels of the isolated molecule. These corrections are obtained for the isolated molecule as the difference between Kohn-Sham HOMO and LUMO eigenvalues and the ionization potential and electron affinity (obtained as total energy differences), respectively. Secondly, a classical image charge model is used to correct the energy levels for screening by the electrodes. Note that the classical image charge model is based on electrostatics and thus neglects any dynamical aspects of the screening process [20].

In the DFT+Σ_{SO} calculations, the DFT energy levels of the molecule in the junction are corrected so as to match the QP energy levels obtained from the GW calculations by a scissor operator (SO):

$$\Sigma_{\mathrm{SO}} = \sum_{\nu \to \mathrm{mol}} \Delta\varepsilon_\nu |\psi_\nu\rangle\langle\psi_\nu|, \tag{3}$$

where the molecular orbitals $|\psi_v\rangle$ are obtained by diagonalizing the DFT Hamiltonian within the subspace spanned by the basis functions of the B4APA. This approach is presented in order to illustrate the effects of the GW self-energy that are beyond the level alignment correction. In this paper, we focus on the dynamical aspects of the screening, which are represented mathematically by the frequency dependence of the GW self-energy.

The transport calculations employ a double ζ with polarization (DZP) basis for all Au atoms, and a double-ζ (DZ) basis for the molecule. We use rather diffuse basis functions for Au corresponding to an energy shift of 0.01 eV. This is necessary to obtain a good description of the surface dipole, which is essential for a correct alignment of molecular energy levels. With the present basis set, we obtain a work function of 5.4 eV for the flat Au(111) surface, in good agreement with the experimental value of 5.3 eV [31].

The conductance and thermopower were calculated from

$$\mathcal{G} = e^2 \mathcal{L}_0(E_F) \tag{4}$$

and

$$\mathcal{S} = \frac{\mathcal{L}_1(E_F)}{eT\mathcal{L}_0(E_F)} = -\frac{\pi^2 k_B^2 T}{3e} \frac{\partial \ln[\mathcal{T}(E)]}{\partial E}\bigg|_{E=E_F}. \tag{5}$$

Here $\mathcal{L}_m(\mu)$ is defined as

$$\mathcal{L}_m(\mu) = \frac{2}{h}\int_{-\infty}^{\infty} dE\, \mathcal{T}(E)(E-\mu)^m \left(-\frac{\partial f(E,\mu,T)}{\partial E}\right), \tag{6}$$

where $f(E,\mu,T)$ is the Fermi-Dirac distribution function. The last expression in $\mathcal{S}$ assumes that the transmission is slowly varying around E_F [11]. T is the average temperature of the left and right electrodes. We note that the thermopower in Eq. (5) is defined within linear response, and is thus applicable when $\Delta T/T$ is small. The nonlinear effects are expected to be of minor importance, since the experiments were done with $T \approx 300$ K and $|\Delta T| < 30$ K. Moreover, the measured thermoelectric current is linearly dependent with small ΔT in the experiments, indicating that the linear response formula is adequate.

III. RESULTS AND DISCUSSION

A. Break junction simulation

To mimic the experimental break junction setup, we stretch the molecular junction by displacing the two Au electrodes in steps of 0.25 Å. The junction is optimized at each displacement step. Figure 2(a) shows the change of the total energy as the junction is stretched. The minimum energy is reached around the configuration $S0$, which represents the zero-stress configuration in the experiments. As shown in Figs. 2(b) and 2(c), the Au-N bond length varies from 2.4 to 2.8 Å, while the angle $\alpha_{\text{Au-N-C}}$ between the Au-N-C atoms changes from 120° to 135°.

The evolution of the conductance and thermopower calculated from DFT and GW is shown in Figs. 2(d) and 2(e), respectively. The DFT conductance remains almost constant, except for the highly stretched configurations. Comparing the DFT conductances with the statistically most probable

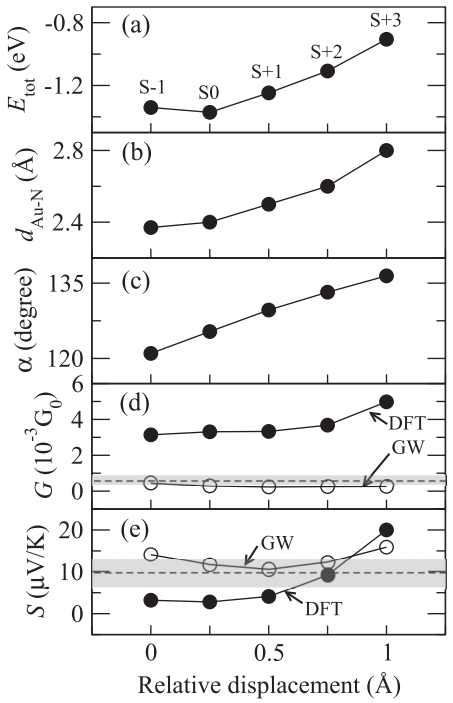

FIG. 2. The effect of stretching the Au/B4APA junction on (a) the total energy, (b) the Au-N bond length $d_{\text{Au-N}}$, (c) the angle $\alpha_{\text{Au-N-C}}$ between the Au-N-C atoms, (d) the conductance, and (e) the thermopower. The statistically most likely conductance 0.57 ± 0.2 ($10^{-3}G_0$) and thermopower 9.7 ± 3 (μV/K) from the break junction experiment are indicated by the gray bars [15]. Each configuration is labeled by $S-1$ to $S+3$ as shown in (a). The relative displacement is scaled to the configuration $S-1$.

experimental conductance indicated by the gray bar, it is clear that the factor of 6 discrepancy cannot be explained by the junction geometry (stretching). For the zero-stress configuration $S0$, the DFT thermopower of 2.8 μV/K is a factor of 3 smaller than the experimental thermopower indicated by the gray bar. The DFT thermopower increases up to 20 μV/K from the configuration $S0$ to the configuration $S+3$. We note that although the DFT thermopower of the configuration $S+2$ is very close to the experimental value, this configuration is considered unlikely in the statistical break junction experiment. Moreover, the DFT conductance of the configuration $S+2$ is a factor of 6 larger than the experimental value. We thus conclude that the large deviation of both the DFT conductance and thermopower from the experimental values cannot be explained to arise from variations in the junction structure.

In contrast to the DFT calculations, the conductance obtained from GW is close to the experimental conductance over a large range of electrode separations. Moreover, the GW thermopower is in overall good agreement with the experimental values, in particular for the low stress configurations.

The variation of the DFT conductance and thermopower during the stretching simulation can be explained by the variation in the HOMO and LUMO positions with respect to the Fermi level. The transmission functions calculated from DFT for the configuration $S0$ to the configuration $S+3$ are shown in Fig. 3. Because the HOMO couples directly to the

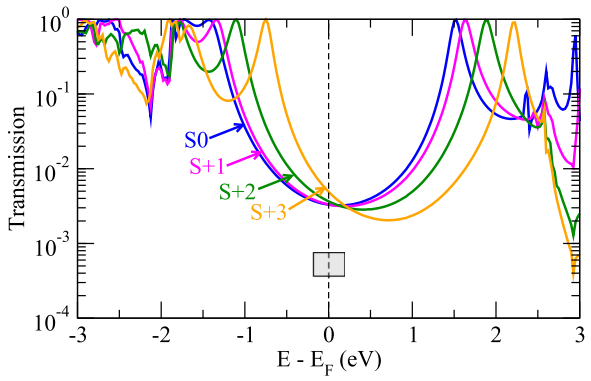

FIG. 3. (Color online) Transmission functions calculated from DFT for the configuration $S0$ to the configurations $S+3$. The gray box indicates the experimental conductance 0.57 ± 0.2 $(10^{-3}G_0)$, and the Fermi level indicated by the dashed line is set to 0 eV [15].

electrodes shown in Fig. 1(b), the coupling strength is reduced when stretching the junction. On the one hand, the reduction of the coupling narrows the HOMO spectral peak from 0.09 to 0.05 eV, fitted from Fig. 3. On the other hand, the charge transfer from the N lone pair to the undercoordinated Au tip atom decreases upon stretching. This effect lowers the magnitude of the local dipole field and shifts the potential on the molecule and thus the molecular energy levels upward in energy.

As the DFT energies of the HOMO and LUMO resonances do not overlap with the characteristic features in the local density of states of the Au $5d$ states around -2 and 2.5 eV, we quantify the change in conductance and thermopower using a simple Lorentzian model [32]. In the case in which the HOMO clearly mediates the transport around E_F, we have

$$\mathcal{T}(E) = \frac{\Gamma^2}{(E-\varepsilon_H)^2+\Gamma^2} \tag{7}$$

and the thermopower is

$$\mathcal{S}_H = -\frac{\pi^2 k_B^2 T}{3e}\frac{2\varepsilon_H}{\varepsilon_H^2+\Gamma^2} \approx -\frac{\pi^2 k_B^2 T}{3e}\frac{2}{\varepsilon_H}. \tag{8}$$

Here Γ is the energy-independent tunneling width and ε_H is the HOMO energy. The last expression assumes that $\varepsilon_H \gg \Gamma$, which is indeed the case as $\varepsilon_H \approx -1$ eV and $\Gamma \approx 0.1$ eV. The thermopower is thus seen to be independent of Γ. This is contrary to the conductance, which approximately is $\mathcal{G} \approx \Gamma^2/\varepsilon_H^2 G_0$, and thus is sensitive to variations in Γ. When stretching the junction, Γ is reduced while the HOMO level moves toward E_F leading to the almost constant conductance seen in Fig. 2(d).

In the case in which both the HOMO and LUMO contribute to the transport, the thermopower is approximately

$$\mathcal{S}_{H+L} \approx -\frac{\pi^2 k_B^2 T}{3e}\left(\frac{2}{\varepsilon_H}+\frac{2}{\varepsilon_L}\right). \tag{9}$$

In the DFT calculations, the low thermopower values are simply due to the fact that the Fermi energy is approximately midway between the HOMO and LUMO energies, i.e., $\varepsilon_H \approx -\varepsilon_L$. For the stretched configuration $S+3$, all the molecular levels are shifted up in energy, and the HOMO is clearly dominating the transport resulting in a higher thermopower.

TABLE I. The HOMO and LUMO energies of the B4APA molecule in the gas phase and in the junction, respectively, calculated from DFT-PBE Kohn-Sham eigenvalues (PBE-eig), GW, HF, and DFT-PBE total energy differences (PBE-tot). Units are eV.

Molecule	Orbital	PBE-eig	GW	HF	PBE-tot
Gas phase	HOMO	−4.4	−5.9	−6.9	−6.3
	LUMO	−1.6	1.2	2.5	0.4
	H-L gap	2.8	7.1	9.4	6.7
Junction	HOMO	−1.4	−2.1	−3.3	N/A
	LUMO	1.5	4.5	6.2	N/A
	H-L gap	2.9	6.6	9.5	N/A

B. Energy levels of molecule in the gas phase

Before investigating the level alignment in the junction, we consider the energy levels in the gas phase. In Table I, the HOMO and LUMO levels in the gas phase are calculated from the PBE Kohn-Sham eigenvalues (PBE-eig), GW, HF, and PBE total energy differences between the neutral and charged molecule (PBE-tot). We have not been able to find experimental data for the ionization potentials or electron affinities of the B4APA. Instead we use PBE total energy differences as a reference, as this approach was found to have an accuracy of around 0.2 eV for the ionization potential of small molecules [33]. Several benchmark studies have established that the accuracy of self-consistent GW for the frontier orbitals of small to intermediate size molecules is 0.3–0.4 eV [33,34].

For the B4APA, the DFT HOMO level is overestimated by 1.9 eV while the DFT LUMO is underestimated by 2.0 eV compared to the PBE-tot. The DFT HOMO-LUMO gap is therefore underestimated by 3.9 eV. These errors are mainly due to the self-interaction errors in the DFT-PBE functional. By using the self-interaction free HF, the gap is opened up to 9.4 eV, which is about 2.7 eV larger than the PBE-tot value. The inclusion of correlation effects at the GW level reduces the HF gap to 7.1 eV, in reasonable agreement with the PBE-tot value of 6.7 eV. In line with the general tendency of self-consistent GW to underestimate molecular ionization potentials [33,34], we find that the HOMO level from the GW calculation lies 0.4 eV above the PBE-tot value.

C. GW transport calculations

In Fig. 4, we compare the transmission functions obtained from DFT, GW, and HF for the zero-stress configuration $S0$. In all calculations, the Fermi level is crossing the tail of the HOMO level signaling a HOMO mediated tunneling process. The transmission features around -2 and 2.5 eV are characteristic features of the local density of states of the Au tip atom. Since the Au atoms are described at the DFT level in all the methods (the self-energy corrections are added only on the molecular subspace), these features are present in all three transmission curves.

The conductances obtained from DFT, GW, and HF are listed in Table II. While DFT (HF) overestimates (underestimates) the conductance by a factor of 6 (26), GW brings the conductance in agreement with the experimental value.

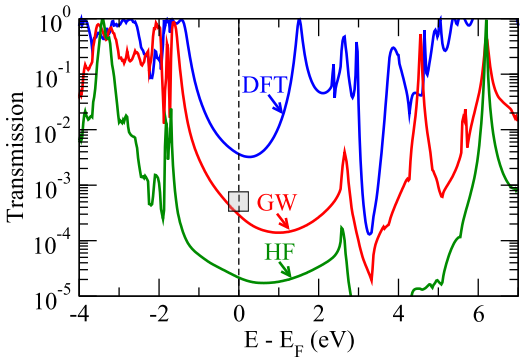

FIG. 4. (Color online) Transmission functions for the zero-stress Au/B4APA junction configuration (S0) calculated from DFT-PBE, GW, and HF. The gray box indicates the experimental conductance 0.57 ± 0.2 ($10^{-3}G_0$), and the Fermi level indicated by the dashed line is set to zero eV [15].

This is a direct result of the more accurate level alignment with respect to the Au Fermi energy. The HOMO and LUMO levels in the junction are listed in the Table I. Due to hybridization, the HOMO-LUMO (H-L) gap in both the DFT and HF calculations is increased by 0.1 eV compared to the gas-phase results. However the H-L gap from GW is *reduced* by 0.5 eV. This reduction of the H-L gap is a consequence of the image charge effect, which is absent in both DFT and HF [17,18].

The thermopowers obtained from DFT, GW, and HF are also shown in Table II. While both DFT and HF underestimate the experimental value by a factor of 3 and 2, respectively, the GW thermopower is in excellent agreement with the experimental value. As noted earlier, the low thermopower obtained from DFT is a consequence of the fact that the Fermi level is positioned in the middle of the HOMO-LUMO gap; see Eq. (9).

D. Dynamical screening

To isolate the role of dynamical effects, we have used a scissors operator to adjust the energies of the molecular orbitals in the DFT calculation to those obtained from GW, see Sec. II. In practice, the energy shifts ($\Delta\varepsilon_\nu$) of the lowest three unoccupied and highest three occupied molecular orbitals are fitted to match the main peaks in the GW transmission spectrum.

In Fig. 5(a), we compare the transmission functions calculated with GW and DFT+Σ_{SO}. It is seen that the full GW transmission is suppressed inside the HOMO-LUMO gap compared to the level matched DFT+Σ_{SO} transmission. At the Fermi level, the GW transmission is a factor of 0.73 lower than the DFT+Σ_{SO} transmission, while the thermopower from the two methods is essentially identical. The reduction of the GW transmission is related to the quasiparticle renormalization factor of the HOMO level, $Z = [1 - d\,\mathrm{Re}\Sigma_H(\varepsilon_H)/dE]^{-1}$. The real part of $\langle\psi_H|\Sigma(E)|\psi_H\rangle$ is shown in Fig. 5(b). The renormalization factor Z describes how well the many-body state representing the molecule with one electron removed from the HOMO can be described as a single particle removed from the neutral ground state. Since the removal of an electron from the molecule will couple to electronic excitations in the electrode via the Coulomb interaction, the stationary states representing the ionized molecule in the junction will contain components where the electrode is in an excited state. For a metal, it is usually valid to describe the response to external fields by a single effective excitation (plasmon pole approximation). The coupling to the plasmon excitation reduces the spectral weight of the HOMO peak, leading to a renormalization factor Z less than unity. For a more detailed discussion of these issues, we refer the reader to Ref. [20].

In the presence of a self-energy, Σ, describing electron-electron interactions, the transmission through a single electronic level coupled to wide band leads can be

TABLE II. Conductance and thermopower for the zero-stress Au/B4APA junction configuration ($S0$) calculated from DFT-PBE, GW, and HF. The experimental values are listed in the last column [15].

	DFT-PBE	GW	HF	Expt.
$\mathcal{G}$ ($10^{-3}G_0$)	3.31	0.29	0.022	0.57 ± 0.2
$\mathcal{S}$ (μV/K)	2.8	11.6	5.4	9.7 ± 0.3

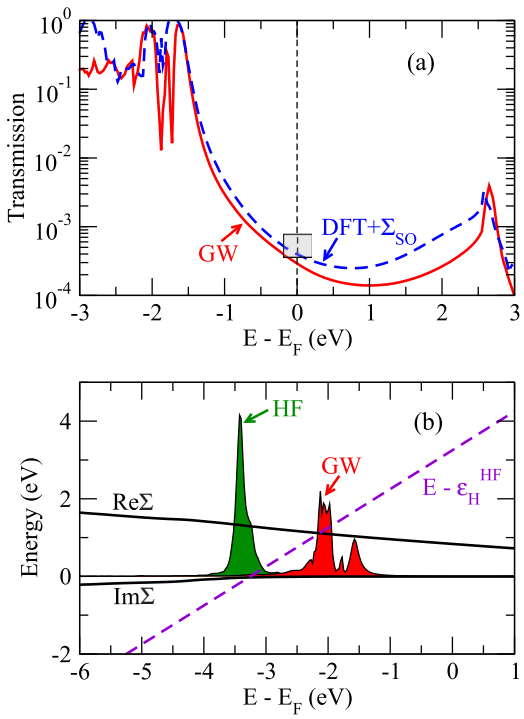

FIG. 5. (Color online) (a) Transmission functions calculated from GW and DFT+Σ_{SO} for the zero-stress Au/B4APA junction configuration ($S0$). In the DFT+Σ_{SO} method, the DFT molecular levels are rigidly shifted to match the GW levels. The gray box indicates the experimental conductance 0.57 ± 0.2 ($10^{-3}G_0$), and the Fermi level indicated by the dashed line is set to 0 eV [15]. (b) The spectral function of the HOMO of the contacted molecule calculated from HF and GW. The real and imaginary parts of the GW self-energy are also shown as black curves.

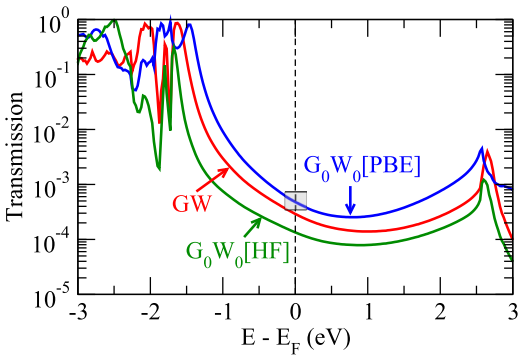

FIG. 6. (Color online) Transmission functions for the zero-stress Au/B4APA junction configuration ($S0$) calculated from G_0W_0 (PBE), self-consistent GW, and G_0W_0 (HF). The gray box indicates the experimental conductance 0.57 ± 0.2 ($10^{-3}G_0$), and the Fermi level indicated by the dashed line is set to 0 eV [15].

written

$$\mathcal{T}^{\mathrm{QP}}(E) = \frac{(Z\Gamma)^2}{\left(E - \varepsilon_a^{\mathrm{QP}}\right)^2 + (Z\Gamma)^2}, \tag{10}$$

where Γ is the (energy-independent) tunneling width and Z is the renormalization factor, and $\varepsilon_a^{\mathrm{QP}}$ is the QP energy level representing the pole of the interacting Green's function. In the off-resonance tunneling regime ($|E - \varepsilon_a^{\mathrm{QP}}| \gg \Gamma$), the conductance becomes

$$\mathcal{G}^{\mathrm{QP}} \approx \frac{(Z\Gamma)^2}{\varepsilon_a^{\mathrm{QP2}}} G_0, \tag{11}$$

which is suppressed by a factor of Z^2 from the level matched noninteracting result. For the HOMO level of 4BAPA in the junction, we find $Z^2 = 0.74$, which agrees almost exactly with the ration between the conductance obtained from GW and DFT+Σ_{SO}.

For the one-level model in the off-resonance regime, the thermopower becomes

$$\mathcal{S}^{\mathrm{QP}} \approx -\frac{\pi^2 k_B^2 T}{3e} \frac{2}{\varepsilon_a^{\mathrm{QP}}}, \tag{12}$$

i.e., independent of Z. This is again consistent with the fact that we find essentially the same thermopower with GW and DFT+Σ_{SO}.

E. One-shot G_0W_0 calculations

To examine the role of self-consistency in the GW calculations, we have performed one-shot G_0W_0 calculations using either DFT-PBE or HF as starting point. The transmission functions obtained from the one-shot G_0W_0 (PBE) and G_0W_0 (HF) calculations are shown in Fig. 6 and the conductances and thermopowers are listed in Table III. Compared to GW, G_0W_0 (PBE) overestimates both the conductance and thermopower while G_0W_0 (HF) underestimates both quantities. These trends can be explained by noting that using DFT-PBE and HF as initial G_0, respectively, overestimates and underestimates the effect of screening (compared to self-consistent GW, which yield energy gaps in between DFT-PBE and HF). As a consequence, the HOMO level is higher with G_0W_0 (PBE) and lower with G_0W_0 (HF). The change in both the conductance and thermopower then follows directly from Eqs. (11) and (12).

TABLE III. The conductance and thermopower for the zero-stress Au/B4APA junction configuration ($S0$) calculated using G_0W_0 (PBE), GW, and G_0W_0 (HF). The experimental values are listed in the last column [15].

	G_0W_0 (PBE)	GW	G_0W_0 (HF)	Expt.
$\mathcal{G}$ ($10^{-3}G_0$)	0.48	0.29	0.13	0.57 ± 0.2
$\mathcal{S}$ (μV/K)	12.9	11.6	9.3	9.7 ± 0.3

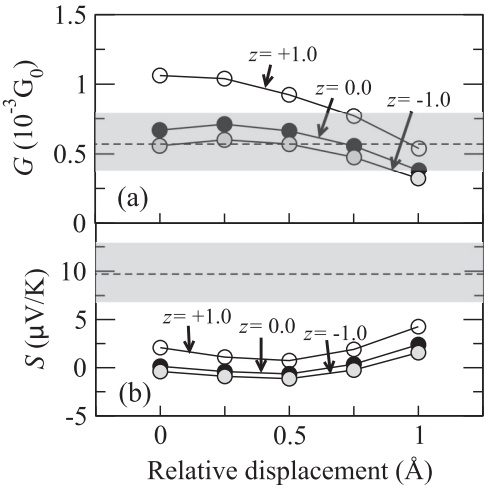

FIG. 7. The effect of stretching the Au/B4APA junction on (a) the conductance and (b) the thermopower, calculated from the DFT+Σ method using three different image plane positions, namely $z = +1, 0, -1$ Å relative to the Au tip atom. The statistically most likely conductance 0.57 ± 0.2 ($10^{-3}G_0$) and thermopower 9.7 ± 3 (μV/K) from the break junction experiment are indicated by the gray bars [15]. The relative displacement is scaled to the configuration $S - 1$.

F. DFT+Σ calculations

Finally, the effect of stretching the Au/B4APA junction on the conductance and thermopower is addressed by using the DFT+Σ method, as shown in Fig. 7. We have employed three different image plane positions, namely $z = +1, 0, -1$ Å relative to the Au tip atom. While the conductances are greatly improved over the uncorrected DFT results, the thermopowers

TABLE IV. Conductance and thermopower for the zero-stress Au/B4APA junction configuration ($S0$) calculated using the DFT+Σ method with three different image plane positions, namely $z = +1, 0, -1$ relative to the Au tip atom. The experimental values are listed in the last column [15].

	+1 Å	0 Å	−1 Å	Expt.
$\mathcal{G}$ ($10^{-3}G_0$)	1.04	0.71	0.60	0.57 ± 0.2
$\mathcal{S}$ (μV/K)	1.1	−0.4	−0.9	9.7 ± 0.3

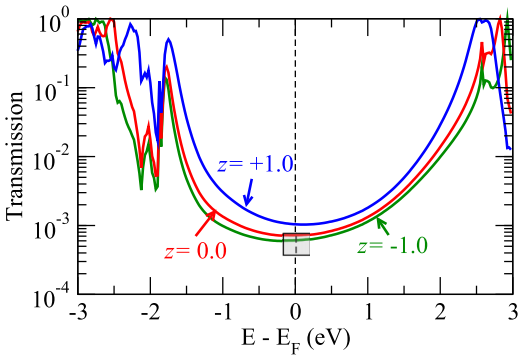

FIG. 8. (Color online) The transmission function for the zero-stress Au/B4APA junction configuration ($S0$) calculated from the DFT+Σ method using three different image plane positions, namely $z = +1, 0, -1$ Å relative to the Au tip atom. The gray box indicates the experimental conductance 0.57 ± 0.2 ($10^{-3} G_0$), and the Fermi level indicated by the dashed line is set to 0 eV [15].

are not improved; in fact they are worsened (see Table IV for the zero-stress configuration).

Contrary to the DFT calculations, where the conductances remains almost constant during the stretching, the conductances are decreased in the DFT+Σ calculations. This is because the image charge effect is reduced when the molecule is moving away from the electrode. As noted earlier, the low thermopowers close to zero are a consequence of the highly symmetric position of the HOMO and LUMO peaks with respect to E_F (see the transmission functions of the zero-stress configuration in Fig. 8).

We note that the DFT + Σ calculations presented in Ref. [15] show an improvement of DFT and a good agreement with the experimental values for both conductance and thermopower. However our configuration $S + 3$ reproduces the DFT and DFT + Σ results reported in Ref. [15], indicating that those calculations were performed for a stretched junction configuration.

IV. CONCLUSIONS

In conclusion, we have demonstrated that the (self-consistent) GW approximation to the electron self-energy provides a quantitatively accurate description of both conductance and thermopower in a gold/bis-(4-aminophenyl) acetylene single-molecule junction. By performing calculations as the junction is pulled apart, it was shown that while the GW approximation yields good agreement with experimental break junction experiments for a large range of electrode separations, the standard DFT description overestimates conductance significantly for all electrode separations and underestimates thermopower for all but the most stretched junction geometries. The main reason for the improved GW description is a better level alignment. However, it was also found that the frequency dependence of the GW self-energy, which accounts for the dynamics of the image charge screening, can have a significant impact on the conductance by reducing the effective metal-molecule coupling strength.

ACKNOWLEDGMENT

The authors acknowledge support from the Danish Council for Independent Research, FTP Sapere Aude Grant No. 11-1051390.

[1] S. V. Aradhya and L. Venkataraman, Nat. Nano. **8**, 399 (2013).
[2] S. Schmaus, A. Bagrets, Y. Nahas, T. K. Yamada, A. Bork, M. Bowen, E. Beaurepaire, F. Evers, and W. Wulfhekel, Nat. Nano. **6**, 185 (2011).
[3] J. Park, A. N. Pasupathy, J. I. Goldsmith, C. Chang, Y. Yaish, J. R. Petta, M. Rinkoski, J. P. Sethna, H. D. Abruna, P. L. McEuen *et al.*, Nature (London) **417**, 722 (2002).
[4] W. Liang, M. P. Shores, M. Bockrath, J. R. Long, and H. Park, Nature (London) **417**, 725 (2002).
[5] P. Sautet and C. Joachim, Chem. Phys. Lett. **153**, 511 (1988).
[6] C. M. Guedon, H. Valkenier, T. Markussen, K. S. Thygesen, J. C. Hummelen, and S. J. van der Molen, Nat. Nanotech. **7**, 305 (2012).
[7] B. O'Regan and M. Grätzel, Nature (London) **353**, 737 (1991).
[8] M. Grätzel, Nature (London) **414**, 338 (2001).
[9] J.-L. Brdas, J. E. Norton, J. Cornil, and V. Coropceanu, Acc. Chem. Res. **42**, 1691 (2009).
[10] K. B. Ørnsø, J. M. Garcia-Lastra, and K. S. Thygesen, Phys. Chem. Chem. Phys. **15**, 19478 (2013).
[11] M. Paulsson and S. Datta, Phys. Rev. B **67**, 241403 (2003).
[12] P. Reddy, S.-Y. Jang, R. A. Segalman, and A. Majumdar, Science **315**, 1568 (2007).
[13] K. Baheti, J. A. Malen, P. Doak, P. Reddy, S.-Y. Jang, T. D. Tilley, A. Majumdar, and R. A. Segalman, Nano Lett. **8**, 715 (2008).
[14] J. A. Malen, P. Doak, K. Baheti, T. D. Tilley, R. A. Segalman, and A. Majumdar, Nano Lett. **9**, 1164 (2009).
[15] J. R. Widawsky, P. Darancet, J. B. Neaton, and L. Venkataraman, Nano Lett. **12**, 354 (2012).
[16] W. Lee, K. Kim, W. Jeong, L. A. Zotti, F. Pauly, J. C. Cuevas, and P. Reddy, Nature (London) **498**, 209 (2013).
[17] J. B. Neaton, M. S. Hybertsen, and S. G. Louie, Phys. Rev. Lett. **97**, 216405 (2006).
[18] J. M. Garcia-Lastra, C. Rostgaard, A. Rubio, and K. S. Thygesen, Phys. Rev. B **80**, 245427 (2009).
[19] M. Strange and K. S. Thygesen, Phys. Rev. B **86**, 195121 (2012).
[20] C. Jin and K. S. Thygesen, Phys. Rev. B **89**, 041102 (2014).
[21] T. Markussen, C. Jin, and K. S. Thygesen, Physica Status Solidi B **250**, 2394 (2013).
[22] J. Enkovaara, C. Rostgaard, J. J. Mortensen, J. Chen, M. Duak, L. Ferrighi, J. Gavnholt, C. Glinsvad, V. Haikola, H. A. Hansen *et al.*, J. Phys.: Condens. Matter **22**, 253202 (2010).
[23] J. P. Perdew, K. Burke, and M. Ernzerhof, Phys. Rev. Lett. **77**, 3865 (1996).
[24] M. Strange, C. Rostgaard, H. Häkkinen, and K. S. Thygesen, Phys. Rev. B **83**, 115108 (2011).
[25] K. S. Thygesen and A. Rubio, Phys. Rev. B **77**, 115333 (2008).
[26] Y. Meir and N. S. Wingreen, Phys. Rev. Lett. **68**, 2512 (1992).
[27] K. S. Thygesen, Phys. Rev. B **73**, 035309 (2006).

[28] A. H. Larsen, M. Vanin, J. J. Mortensen, K. S. Thygesen, and K. W. Jacobsen, Phys. Rev. B **80**, 195112 (2009).
[29] D. J. Mowbray, G. Jones, and K. S. Thygesen, J. Chem. Phys. **128**, 111103 (2008).
[30] S. Y. Quek, L. Venkataraman, H. J. Choi, S. G. Louie, M. S. Hybertsen, and J. B. Neaton, Nano Lett. **7**, 3477 (2007).
[31] H. B. Michaelson, J. Appl. Phys. **48**, 4729 (1977).
[32] T. Kim, P. Darancet, J. R. Widawsky, M. Kotiuga, S. Y. Quek, J. B. Neaton, and L. Venkataraman, Nano Lett. **14**, 794 (2014).
[33] C. Rostgaard, K. W. Jacobsen, and K. S. Thygesen, Phys. Rev. B **81**, 085103 (2010).
[34] X. Blase, C. Attaccalite, and V. Olevano, Phys. Rev. B **83**, 115103 (2011).